BIOCHEMISTRY
including biophysical chemistry & molecular biology
Article

Biochemistry **2010,** *49,* 8187–8196 8187
DOI: 10.1021/bi100802k

Direct Measurement of Mercury(II) Removal from Organomercurial Lyase (MerB) by Tryptophan Fluorescence: NmerA Domain of Coevolved γ-Proteobacterial Mercuric Ion Reductase (MerA) Is More Efficient Than MerA Catalytic Core or Glutathione[†,‡]

Baoyu Hong,[§] Rachel Nauss,[§] Ian M. Harwood,[∥] and Susan M. Miller*[,§,∥]

[§]*Department of Pharmaceutical Chemistry and* [∥]*Graduate Group in Biophysics, University of California San Francisco, San Francisco, California 94158-2517*

Received May 19, 2010; Revised Manuscript Received August 17, 2010

ABSTRACT: Aerobic and facultative bacteria and archaea harboring *mer* loci exhibit resistance to the toxic effects of Hg(II) and organomercurials [RHg(I)]. In broad spectrum resistance, RHg(I) is converted to less toxic Hg(0) in the cytosol by the sequential action of organomercurial lyase (MerB: RHg(I) → RH + Hg(II)) and mercuric ion reductase (MerA: Hg(II) → Hg(0)) enzymes, requiring transfer of Hg(II) from MerB to MerA. Although previous studies with γ-proteobacterial versions of MerA and a nonphysiological Hg(II)−DTT−MerB complex qualitatively support a pathway for direct transfer between proteins, assessment of the relative efficiencies of Hg(II) transfer to the two different dicysteine motifs in γ-proteobacterial MerA and to competing cellular thiol is lacking. Here we show the intrinsic tryptophan fluorescence of γ-proteobacterial MerB is sensitive to Hg(II) binding and use this to probe the kinetics of Hg(II) removal from MerB by the N-terminal domain (NmerA) and catalytic core C-terminal cysteine pairs of its coevolved MerA and by glutathione (GSH), the major competing cellular thiol in γ-proteobacteria. At physiologically relevant concentrations, reaction with a 10-fold excess of NmerA over HgMerB removes ≥92% Hg(II), while similar extents of reaction require more than 1000-fold excess of GSH. Kinetically, the apparent second-order rate constant for Hg(II) transfer from MerB to NmerA, at $(2.3 \pm 0.1) \times 10^4\ M^{-1}\ s^{-1}$, is ∼100-fold greater than that for GSH ($(1.2 \pm 0.2) \times 10^2\ M^{-1}\ s^{-1}$) or the MerA catalytic core ($1.2 \times 10^2\ M^{-1}\ s^{-1}$), establishing transfer to the metallochaperone-like NmerA domain as the kinetically favored pathway in this coevolved system.

Oxidized forms of mercury, mercuric ions Hg(II)[1] and organomercurial compounds RHg(I) (e.g., methylmercury MeHg(I)), are well-known for their high toxicity to living organisms (*1*, *2*). Underlying the toxicity is their formation of high-affinity ($K_{formation}$ for $Hg(SR)_2 \sim 10^{38}$ to $10^{45}\ M^{-2}$ (*3*)) but rapidly exchangeable complexes with thiols (*2*−*4*). When they enter cells, these properties lead both to depletion of the cellular pool of thiol redox buffer molecules (e.g., glutathione, GSH, in eukaryotes and γ-proteobacteria) and to exchange of Hg(II) and RHg(I) onto cysteine thiols of many proteins causing a pleiotropic loss of function (*2*). Since neutral complexes (e.g., $HgCl_2$ and MeHgCl) can diffuse through membranes and charged complexes (e.g., MeHgS-Cys, $Hg(S\text{-}Cys)_2$) can be imported fortuitously by various transporters, such as organic anion transporters (*5*, *6*), their entry into cells is inevitable. As a result, evolved mechanisms of mercury resistance rely on intracellular processes to sequester and eliminate these toxins.

In the widespread mechanism for resisting mercury toxicity encoded by *mer* loci in aerobic and facultative bacteria, resistance is ultimately afforded by enzyme (mercuric ion reductase, MerA) catalyzed reduction of Hg(II) to elemental mercury that simply diffuses out of the cell and dissipates (*7*). But maximal narrow spectrum resistance to Hg(II) also requires the presence of integral membrane proteins (e.g., MerT) that actually facilitate Hg(II) uptake, and broad spectrum resistance to RHg(I) requires an additional cytoplasmic enzyme (organomercurial lyase, MerB) that catalyzes protonolysis of the C−Hg bond in RHg(I) to generate Hg(II) for reduction by MerA (*7*). With this deliberate operon-encoded transport of Hg(II) into and production of Hg(II) from RHg(I) within the cytoplasm, a mechanism for direct handoff of Hg(II) from the Hg(II)-source proteins, MerT and MerB, to the detoxifier MerA is expected to have evolved to minimize further distribution of Hg(II) to other cellular proteins and maximize the efficiency of detoxification (*8*). Such a strategy involving dicysteine-containing motifs in partner proteins is now well documented for other thiophilic metal trafficking pathways, particularly for Cu(I) (*9*−*11*). For the *mer* pathway, however, explicit evidence for direct transfer between intact *mer* pathway proteins in the absence of competing thiols is limited to direct measurement of Hg(II) transfer between the CXXC dicysteine motif in the separately expressed, well-folded N-terminal domain (NmerA) (*12*) from the narrow spectrum γ-proteobacterial Tn*501* MerA and the CCAG dicysteine motif in the C-terminal tail of its separately expressed catalytic core (*13*, *14*). Whether either of these motifs directly accesses Hg(II) from integral

[†]This work was supported by the Office of Science (BER), U.S. Department of Energy, Grants DE-FG02-05ER64120 and DE-FG02-07ER64409.

[‡]GenBank accession number GU062788 for the complete nucleotide sequence for the pDU1358 *merA* gene.

*Address correspondence to this author. Tel: 415-476-7155. Fax: 415-502-8298. E-mail: smiller@cgl.ucsf.edu.

[1]Abbreviations: MerB, organomercurial lyase; MerA, mercuric ion reductase; NmerA, N-terminal domain of mercuric ion reductase; DTT, dithiothreitol; GSH, glutathione; IPTG, isopropyl β-D-thiogalactoside; Hg(II), mercuric ion; RHg(I), organomercurial ion; $Hg(SG)_2$, mercuric diglutathione; FAD, flavin adenine dinucleotide; NADPH, reduced nicotinamide adenine dinucleotide phosphate.

Published on Web 08/19/2010

membrane MerT is still unresolved, but NmerA has been shown to efficiently scavenge Hg(II) from a peptide based on an intracellular loop of MerT (*15*), and bacterial two-hybrid studies suggest some type of protein−protein interaction between MerA and MerT does occur within cells (*16*).

Two studies with γ-proteobacterial versions of MerB and MerA qualitatively support a pathway for direct transfer from MerB to MerA (*17*, *18*). In the first, an undefined amount of MerA was reported to provide 6−7-fold enhancement of steady-state turnover by partially purified MerB, but interpretation of the result is limited by the observation that bovine serum albumin included in the assays also enhanced the activity by 3−5-fold (*17*). In the second study, protein buffering assays using varied concentrations of MerB at a single concentration of competing cysteine provided evidence that MerA could directly acquire Hg(II) at a low rate from a DTT−Hg(II)−MerB complex (*18*). However, the nonphysiological DTT−Hg(II)−MerB complex is unusually stable and inhibited in normal steady-state assays of MerB that use cysteine or glutathione to release Hg(II) during turnover. Thus use of this DTT−Hg(II)−MerB complex provides little insight into the relative efficiencies of competing pathways for Hg(II) transfer from the physiologically relevant Hg(II)−MerB product complex to MerA versus the major γ-proteobacterial buffer thiol molecule glutathione (*18*). In addition, the use of apparently full-length MerA (with very low reported activity of ∼5% suggesting significant thiol oxidation) precluded identification of which dicysteine motif of MerA initiates the transfer (*18*).

In this regard, previous studies have shown the separately expressed NmerA domain from γ-proteobacterial Tn*501* MerA is structurally well-folded (*12*, *19*), is much more efficient than the catalytic core or glutathione at scavenging Hg(II) from cellular proteins (*13*), and enhances in vivo resistance of glutathione-depleted cells to Hg(II) (*13*). These results suggest that the NmerA CXXC site in broad spectrum γ-proteobacterial MerAs may also be the primary site for direct transfer of Hg(II) from their coevolved MerBs. The goal of the present work is to test this hypothesis by quantifying the relative efficiency of the three most likely physiological pathways for Hg(II) transfer between coevolved γ-proteobacterial MerB and MerA proteins: (1) transfer via cellular thiol glutathione, (2) direct transfer to the CXXC site in the NmerA domain, and (3) direct transfer to the CCAG site in the catalytic core. To address this, we have cloned the separate NmerA and catalytic core domains of the MerA from the broad spectrum *mer* operon on the γ-proteobacterial pDU1358 plasmid (*20*) and have evaluated the kinetics of Hg(II) transfer from the well-characterized γ-proteobacterial R831b MerB (*21*−*25*) that differs by only one amino acid from the coevolved pDU1358 MerB to each of these domains and to glutathione by monitoring either changes in the MerB intrinsic tryptophan fluorescence, which we have shown is sensitive to Hg(II) binding, or changes in the flavin fluorescence of the catalytic core (*14*).

EXPERIMENTAL PROCEDURES

Cloning and Expression of pDU1358 NmerA Domain and Core MerA. Plasmid pDU1358, which was originally isolated from *Serratia marcescens* and harbors a broad resistance *mer* operon (*20*), was a generous gift from Dr. Anne O. Summers. The 210 bp fragment corresponding to the 69-residue NmerA domain (see Figure 1) was PCR-amplified using forward (5′ GGGAATTC**CATATG**ACCCATCTAAAAATCACCGGC 3′) and reverse (5′ GGC**GGATCC**CTATGCATCGGCGAGCATCGCTTTG 3′) primers designed to introduce an *Nde*I site, a stop codon, and a *Bam*HI site (respectively, in bold). The PCR fragment was incorporated into a pET3a vector to generate pET3a:pDUNmerA, transformants of XL-10 *Escherichia coli* were selected on LB/ampicillin (50 μg/mL) plates, and genes were verified by DNA sequencing. DNA coding for catalytic core MerA (E96−G561; see Figure 1) was PCR-amplified using forward (5′ GCATCT**CCATGG**AGCGCCCGTTGCAAGTCGC 3′) and reverse (5′ CGA**GGATCC**TGGGGCGAGCTTCATGGTTCCAT 3′) primers designed to incorporate a start codon with an *Nco*I site prior to the E96 codon and a *Bam*HI site after the stop codon (respectively, in bold). The ∼1400 bp fragment was ligated into a TOPO-TA vector and transformed into *E. coli* Top 10 competent cells. Transformants were selected from kanamycin plates (50 μg/mL), and the gene was verified by DNA sequencing. The verified construct was incorporated into a pET11d vector after sequential digestion of both with *Nco*I and *Bam*HI to yield pET11d:pDUcore. XL-1 Blue *E. coli* transformants were selected on ampicillin (50 μg/mL) plates and reverified by DNA sequencing.

Protein Preparations. The pDU1358 MerA catalytic core [mercury(II) reductase, EC 1.16.1.1] and NmerA proteins were prepared as previously described for the Tn*501* proteins (*13*) with one exception: NmerA, which has one more negative charge than Tn*501* NmerA (Asp45 vs Val, Figure 1), remained bound to the tandem DEAE and Fast-Q anion-exchange columns. After a 300 mL wash, the protein was eluted with a linear gradient of 0−500 mM NaCl in a total of 400 mL of Tris-HCl buffer, pH 8.0. Plasmid pQZB1, which carries the R831b MerB gene (*25*), was a generous gift from Dr. Anne O. Summers. MerB (organomercurial lyase, EC 4.99.1.2) was expressed and purified as previously described (*13*, *25*). All proteins were judged ≥95% pure by SDS−PAGE and were stored at −80 °C in the presence of 10% glycerol.

Prior to use, all proteins were incubated with dithiothreitol (DTT) (10 mM for NmerA and MerB, 5 mM for core) at room temperature for 30 min and then separated from DTT and exchanged into 50 mM potassium phosphate (KP_i), pH 7.3, by gel filtration chromatography using Bio-Gel P2 (Bio-Rad) resin for NmerA, Bio-Gel P6 (Bio-Rad) for MerB, and Sephadex G25 for core. Protein concentrations were calculated using ε_{278nm} = 2.55 mM^{-1} cm^{-1} for NmerA (*13*), ε_{280nm} = 23.95 mM^{-1} cm^{-1} for MerB (*25*), and ε_{456nm} = 11.3 mM^{-1} cm^{-1} for MerA catalytic core active sites (*26*), respectively. Thiol titrations were performed under denaturing conditions as previously described (*13*, *25*) to confirm appropriate number of reduced thiols for each protein [2 for NmerA, 4 for MerB, and 4 for MerA core (two adjacent to FAD remain as disulfide in core (*27*))].

Steady-State Assays of pDU1358 Core MerA. Initial rates were measured in triplicate at 25 °C in 50 mM KP_i, pH 7.3, using a saturating concentration (50 μM) of NADPH (Sigma, N-1630), 50 nM MerA core (active sites), and varied concentrations (5−250 μM) of either $Hg(SG)_2$ in the presence of 1 mM unliganded GSH or pDU1358 HgNmerA alone as substrate. Each concentration of $Hg(SG)_2$ was generated in situ by addition of $HgBr_2$ (ACS reagent) and sufficient GSH (Sigma, ≥98%) in excess of 1 mM to form the dithiol complex. The 1:1 stoichiometric complex of HgNmerA was generated by titration of NmerA with 1.0 equiv of Hg(5-thio-2-nitrobenzoate)$_2$ as previously described (*13*). Initial velocity data were fit to the Michaelis−Menten equation using the curvefit routines in Kaleidagraph: $v/E_T = k_{cat}[\text{Hg-dithiol}]/(K_{MHg} + [\text{Hg-dithiol}])$, where v is the initial velocity and E_T is the enzyme active site concentration. Errors in k_{cat} and K_{MHg} are from the fitting analysis. Alternatively, to

determine errors in k_{cat}/K_{MHg}, the data were fit to the alternative form of the equation: $v/E_T = ((k_{cat}/K_{MHg})[\text{Hg-dithiol}])/((k_{cat}/(k_{cat}/K_{MHg})) + [\text{Hg-dithiol}])$ (*28*).

Titration of MerB with Hg(II) Monitored by Tryptophan Fluorescence. Changes in MerB intrinsic tryptophan fluorescence during titration of 5 μM MerB in 50 mM KP_i, pH 7.3, at 25 °C with $HgBr_2$ were recorded using a Jobin Yvon Fluorolog-3 spectrofluorometer with λ_{ex} = 280 nm and λ_{em} = 340 nm. In a separate experiment, MerB was titrated with $HgBr_2$ up to 1.0 equiv after which NmerA was added to a final concentration of 350 μM, and emission spectra were recorded using λ_{ex} = 295 nm to avoid inner filter effects from NmerA. All spectra/values were corrected for dilution. In control experiments, no change in fluorescence was observed upon addition of unliganded NmerA to unliganded MerB, nor upon addition of HgNmerA to HgMerB.

Stopped-Flow Analysis. Single mixing mode of a HiTech SF-61DX2 (TgK Scientific Ltd., U.K.) stopped-flow apparatus was used for all kinetic measurements. All reactions were performed in 50 mM KP_i buffer, pH 7.3, with temperature control at 25 °C. Fluorescence data were collected in single beam mode with photomultiplier detection. Pseudo-first-order conditions were maintained for all measurements. The HgMerB complex was made by titration of MerB with 1 equiv of $HgBr_2$ and the 1:1 stoichiometry verified by electrospray mass spectrometry using an ABI QSTAR XL spectrometer at the UCSF Mass Spectrometry facility (supported by NIH NCRR P41RR001614). For measurement of Hg(II) transfer from HgMerB to either NmerA or GSH, equal volumes of 10 μM HgMerB and varied concentrations of the appropriate thiol were mixed in the stopped flow, and Hg(II) release was monitored by changes in the MerB tryptophan fluorescence using an excitation wavelength of 295 nm to avoid inner filter effects of varied NmerA concentrations and an emission filter with a 320 nm cutoff. For measurement of Hg(II) transfer from HgMerB to the MerA catalytic core, equal volumes of 10 μM MerA core and varied concentrations of HgMerB were mixed in the stopped flow, and Hg(II) transfer was monitored by changes in the MerA flavin fluorescence using an excitation wavelength of 445 nm and an emission filter with a 455 nm cutoff (*14*). Control reactions with 20 mM GSH for the GSH and NmerA experiments and with 100 μM $Hg(SG)_2$ for the MerA core experiments were used to set the voltage for detection of maximal fluorescence. All kinetic traces used in analysis represent an average of three to five individual traces. Raw data were fit to single or double exponential equations using the software provided with the instrument according to eq 1:

$$F(t) = F(\infty) - \sum_{i=1}^{2} A_i \exp(-k_i t) \quad (1)$$

where $F(t)$ is relative fluorescence intensity at time t, $F(\infty)$ is the fluorescence intensity at time infinity, A_i is the amplitude of the ith phase, and k_i is the observed rate constant characterizing the ith phase (i = 1 or 2). The concentration dependence of the rate constants in each case were fit either to a linear expression for a simple second-order process or to eq 2 corresponding to the minimal two-step model in Scheme 1, where B = NmerA or GSH and $K_{1/2} = (k_{max} + k_2)/k_1$ (*29*).

$$k_{obs} = \frac{k_{max} B}{K_{1/2} + B} + k_{rev} \quad (2)$$

Global Kinetic Modeling. The software program Berkeley Madonna X (Mach-O) v.8.3.21 (www.berkeleymadonna.com) was used for simulations and global fitting of models to the kinetic traces for the reactions of HgMerB with NmerA (Scheme 2) and GSH (Scheme 3). As indicated for both models, all MerB species with Hg(II) bound to Cys96 were assumed to have the same partially quenched fluorescence as the initial HgMerB complex, while all species without Hg(II) bound to Cys96 were assumed to have the full fluorescence of unbound MerB. In both cases total fluorescence as a function of time was calculated as the sum of the "low fluorescence" species multiplied by the starting fluorescence plus the sum of the "high fluorescence" species multiplied by the final high fluorescence of unbound MerB determined in the control reactions. For modeling of the NmerA data according to Scheme 2, the initial HgMerB was set equal to species A + species A′, and the concentrations of A and A′ were allowed to vary between 80−100% and 0−20%, respectively, of the total 5 μM concentration. In the final fit, A′ averaged 16 ± 1.8% over the five conditions. As noted below no separate slow phase was observed in the GSH reactions, so no separate path for reaction of GSH with A′ was included in Scheme 3.

RESULTS AND DISCUSSION

R831b MerB and pDU1358 MerA Are Suitable as "Coevolved" Enzymes. The R831b MerB (from γ-proteobacterium *S. marcescens*, GenBank accession number U77087 (*30*, *31*)) used in previous steady-state studies (*17*, *18*) is structurally and mechanistically well characterized (*21*−*25*, *32*), but it was cloned (*25*) from an organomercurial resistance locus that retains only remnants of its coevolved MerA (*31*, *33*). Nonetheless, it is entirely suitable for this study as it differs by only one amino acid (L10R) from MerB in the intact pDU1358 broad spectrum resistance locus (also from *S. marcescens*, GenBank accession number M15049 (*20*)). The coevolved pDU1358 MerA (GenBank accession number GU062788) is ~91% identical to the well-characterized narrow spectrum Tn*501* MerA (GenBank accession number Z00027 (*34*), Figure 1), but has several significant differences in polarity and charge (black highlights in Figure 1) in residues on potential interaction surfaces in the two domains (core PDB ID 1ZK7 (*13*, *19*); NmerA PDB ID 2KT2 (Ledwidge et al., submitted) and (MerAa) structure reported in ref *19*). To ensure optimal interactions we cloned and expressed the corresponding pDU1358 NmerA and catalytic core components shown in Figure 1.[2] Note that the structurally conserved catalytic core has two essential pairs of cysteines, one deeply buried pair (Cys136, Cys141) that binds Hg(II) at the site of FAD-mediated reduction by NADPH and a second pair on the flexible C-terminus of the protein (Cys558, Cys559) that is the essential entry point for Hg(II) into the core. This latter pair rapidly displaces thiol ligands from incoming Hg-dithiol substrates such as $Hg(SG)_2$ (SG = glutathione) or the Hg(II) complex of NmerA (*14*) and passes the Hg(II) to the buried active site cysteines for reduction (*7*, *35*). This C-terminal pair is the only set of MerA cysteines available for direct interaction of core with MerB. Steady-state assays with the pDU1358 catalytic core at pH 7.3 yield slightly lower k_{cat} and k_{cat}/K_{MHg} values than previously observed for the Tn*501* catalytic core (*13*) (Table 1). However, the values obtained using $Hg(SG)_2$ as the substrate in

[2]We also cloned the full-length pDU1358 MerA but did not examine its interaction with HgMerB in part because this protein, as with all MerA proteins studied, undergoes partial in vivo proteolytic removal of the N-terminal domain but primarily because the main goal of these studies was to identify which component yields the most efficient transfer of Hg(II) to MerA.

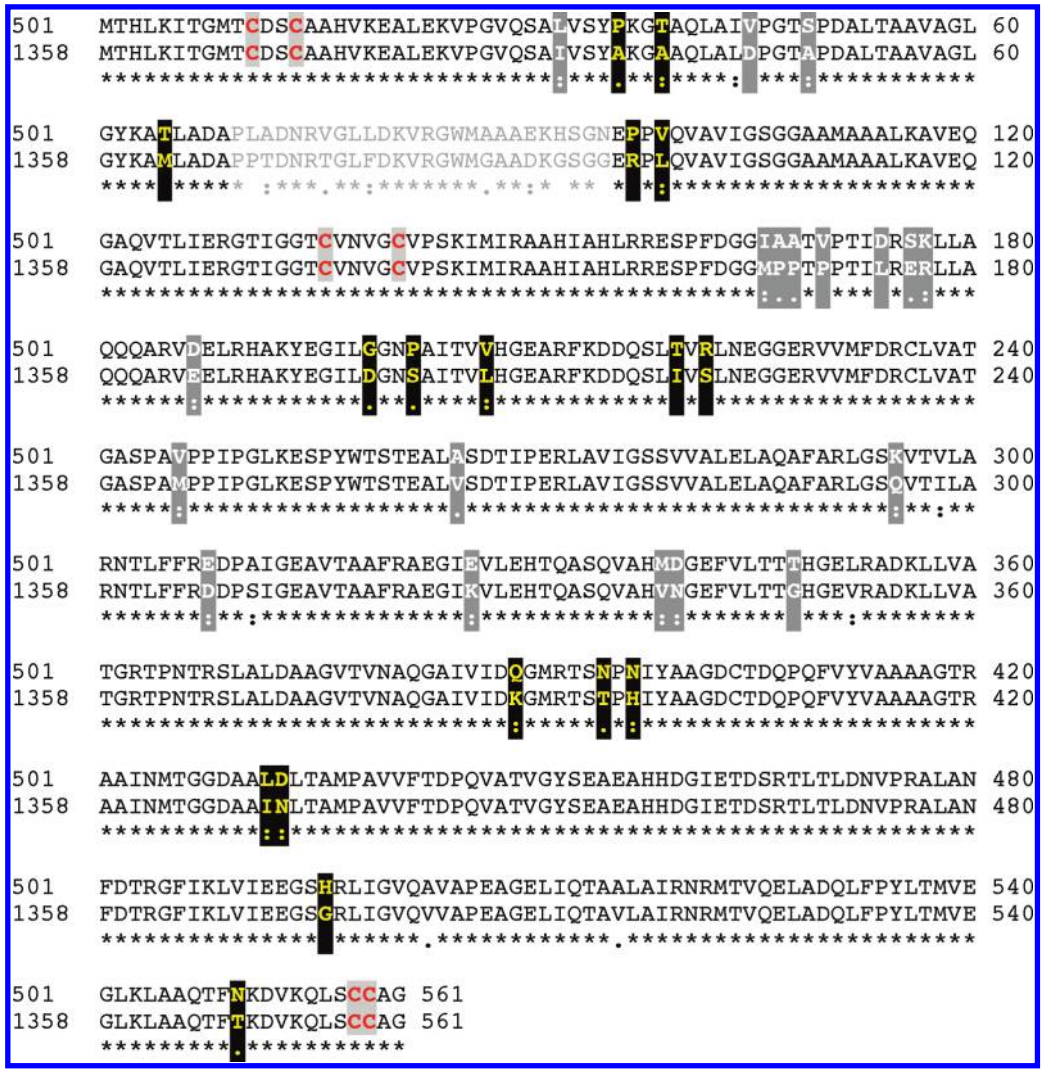

FIGURE 1: Most significant amino acid differences between Tn*501* and pDU1358 MerA occur on surfaces. Clustal W2 (version 2.0.11; http://www.ebi.ac.uk/Tools/es/cgi-bin/clustalw2/) alignment of MerA sequences from well-characterized narrow spectrum Tn*501* operon (GenBank accession number Z00027; MerA core PDB ID 1ZK7; NmerA PDB ID 2KT2) and broad spectrum pDU1358 operon (GenBank accession number GU062788). NmerA domain (residues 1−69) and catalytic core (residues 96−561) (*13*) sequences are in black with surface variations highlighted; linker region (residues 70−95) sequence is in pale gray. Black highlights/yellow letters, surface residues most likely to interact with MerB; gray highlights/white letters, other surface residues more remote from potential interacting dicysteine motifs; light gray highlights/red letters, Hg(II)-binding (Cys11, Cys14, Cys558, Cys559) and catalytic (Cys136, Cys141) cysteines.

Table 1: Steady-State Kinetic Constants for pDU1358 and Tn*501* MerA Catalytic Core[a]

	pDU1358 MerA[b]			Tn*501* MerA[c]		
substrate	k_{cat} (s^{-1})	k_{cat}/K_{MHg} (M^{-1} s^{-1} × 10^5)	K_{MHg} (μM)	k_{cat} (s^{-1})	k_{cat}/K_{MHg} (M^{-1} s^{-1} × 10^5)	K_{MHg} (μM)
$Hg(SG)_2$ + 1 mM GSH	7.7 ± 0.1	1.2 ± 0.1	63.0 ± 3.2	8.7 ± 0.1	3.6 ± 0.2	24.0 ± 1.0
HgNmerA[d]	7.7 ± 0.7	0.89 ± 0.18	87.0 ± 15.4	12.0 ± 0.3	3.4 ± 0.3	35.1 ± 3.3

[a]Conditions as described in Experimental Procedures. [b]This work. [c]Ledwidge et al. (*13*). [d]Tn*501* HgNmerA was used as substrate for Tn*501* core MerA, and pDU1358 HgNmerA was used as substrate for pDU1358 core MerA.

the presence of 1 mM glutathione are nearly identical to those obtained using its own HgNmerA as substrate in the absence of glutathione, which is similar to the behavior observed for the Tn*501* catalytic core (*13*) (Table 1).

MerB Intrinsic Tryptophan Fluorescence Is Sensitive to Hg(II) Binding. Figure 2 shows the overall structure and a close-up of the active site of the Hg(II) product complex of R831b MerB (PDB ID 3FN8 (*24*, *32*)). Of the three cysteines shown, Cys96 and Cys159 are essential catalysts of C−Hg protonolysis (*25*). Cys160, which is conserved in γ-proteobacterial MerBs but is not universally conserved in all MerBs, is not essential for C−Hg cleavage but may play a role in RHg(I) binding and Hg(II) release (*25*). The close proximity of Trp95 to the Hg(II) product chelated by Cys96 and Cys159 in the active site (Figure 2B) suggested Trp fluorescence as a possible probe for Hg(II) binding and release from the active site. Since identical Hg(II)−product complexes were observed in crystals obtained from turnover of RHg(I) soaked into the crystal (PDB ID 3F0P (*24*)) and from

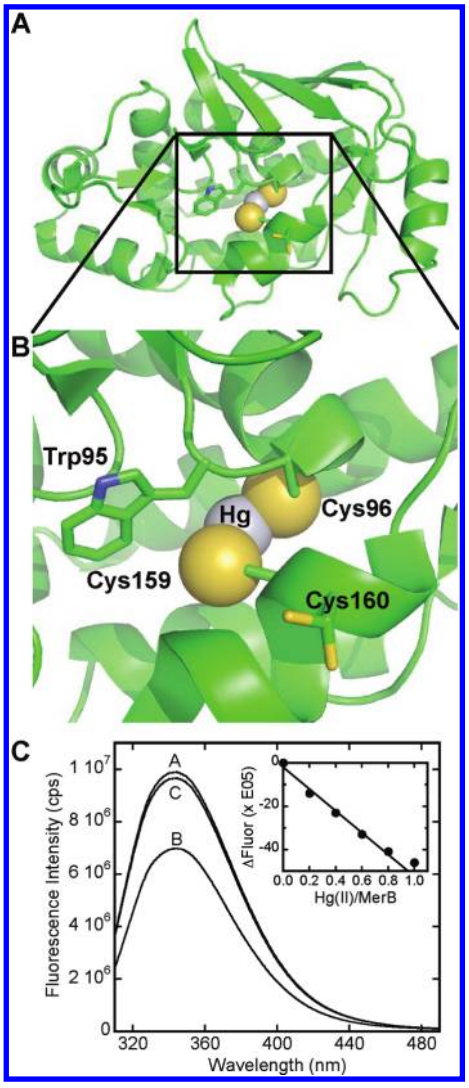

FIGURE 2: MerB tryptophan fluorescence is sensitive to Hg(II) binding. (A) Overall structure of HgMerB and (B) close-up of active site (PDB ID 3FN8 (*32*)) showing the position of Trp95 relative to Hg(II) bound to Cys96 and Cys159 at the catalytic site and Cys160 that may be involved in Hg(II) transfer. Electron density for Cys160 indicates it adopts two conformations in the crystal structures (*24*, *32*). (C) Changes in MerB intrinsic tryptophan fluorescence upon binding/release of Hg(II) at 25 °C. Normalized spectra obtained with λ_{ex} = 295 nm are for MerB (5 μM) (spectrum A), MerB + 1.0 equiv of $HgBr_2$ (spectrum B), HgMerB after addition of 350 μM NmerA (spectrum C). Inset: Changes in fluorescence emission at 340 nm with λ_{ex} = 280 nm. Off-peak excitation at 295 nm was used for spectra comparing effect of NmerA to avoid inner filter effects of absorbance by NmerA at 280 nm.

Hg(II)-titrated MerB (PDB ID 3FN8, personal communication (*32*)), we chose to make the HgMerB complex by titration for simplicity. Titration of MerB with 1.0 equiv of $HgBr_2$ leads to a linear decrease in Trp fluorescence intensity through ~0.9 equiv (Figure 2C), and this is reversed by ≥90% upon addition of excess NmerA but not by addition of the HgNmerA complex. Likewise, no change in fluorescence was observed upon addition of NmerA to unliganded MerB, indicating the fluorescence change is specifically associated with the binding/removal of Hg(II) from the active site and that this is an ideal probe for monitoring the kinetics of Hg(II) removal by various thiols.

Since previous NMR structural studies of HgMerB suggested it may be unstable (*23*), we evaluated the stability of our 1:1 HgMerB complex in comparison with MerB using HPLC size exclusion chromatography (Supporting Information Figure S1). Analysis immediately after mixing MerB with $HgBr_2$ shows a major peak (80−85%) eluting with a retention time similar to that of monomeric MerB and a minor peak eluting at shorter times corresponding to slightly less than the dimeric molecular weight. This smaller peak increases slowly, reaching ~25% at 2 h. In the stopped-flow experiments described below, all data were collected in ≤1 h after mixing to limit the presence of this alternative (possibly dimeric) species during the kinetic analysis.

To verify that the return of MerB fluorescence is due to direct transfer of Hg(II) from HgMerB to NmerA, we mixed HgMerB and NmerA in a 1:1 molar ratio, separated and collected fractions for the MerB/HgMerB and NmerA/HgNmerA peaks using HPLC size exclusion chromatography (Supporting Information Figure S2), and analyzed the two fractions by electrospray ionization mass spectrometry. As shown in Supporting Information Figure S3, mass spectra for both protein fractions contain both the apo and the Hg-bound forms verifying the return of fluorescence results from removal of Hg(II) from HgMerB by NmerA and can be used to monitor the kinetics of this process.

For measurement of rates of Hg(II) removal from HgMerB by NmerA or glutathione (GSH), we monitored the change in MerB fluorescence with the final concentration of HgMerB fixed at 5 μM and the NmerA and GSH concentrations varied as noted in panels A and B of Figure 3, respectively, to maintain pseudo-first-order conditions. The traces for NmerA fit best to a double exponential equation (i = 2 in eq 1) with a major fast phase (amplitude ~85%) and a minor slow phase. The behavior of the fast phase (k_{obs}) was dependent on NmerA concentration as discussed below. The observed rate constants for the slow phase, k_s, were independent of NmerA concentration with an average value of ~0.4 s^{-1}. Since this is slower than measured rates of steady-state turnover of MerB and the ~15% amplitude of this phase is consistent with the estimated amounts of the faster eluting peak in the chromatography (Supporting Information Figure S1), we suspect this phase represents a rate-limiting conversion of that minor species to a form that reacts more rapidly with NmerA and treat it as a side reaction in our analysis. The traces for GSH fit well to a single exponential, with the exception of an additional very minor second linear phase (~0.05 ΔFluor/s) observed only at the highest two GSH concentrations. Since the exponential phase here accounts for >97% of the amplitude at these concentrations, the linear phase is inconsequential and was not analyzed further.

NmerA Reacts More Completely Than Glutathione (GSH) with HgMerB. Comparing the traces in Figure 3A,B for NmerA and GSH, one striking difference is immediately apparent. In Figure 3A, all but one trace for the lowest concentration of NmerA proceed to the same fluorescence end point that is essentially the same as that of unliganded MerB, indicating the equilibrium for transfer of Hg(II) to NmerA lies highly in favor of HgNmerA with as little as a 10-fold excess of NmerA over MerB. In contrast, the end points in Figure 3B vary dramatically with GSH concentration, indicating a much less favorable equilibrium for transfer of Hg(II) from HgMerB to GSH. This difference in equilibrium properties is consistent with the fact that GSH is a monothiol compound and hence requires 2 equiv to fully extract Hg(II) from HgMerB, while NmerA has evolved with a dithiol perfectly positioned to chelate Hg(II) at much lower total thiol concentrations. Further examination of the GSH equilibria are described below.

Lower Concentrations of NmerA Acquire Hg(II) Faster Than GSH. The second difference to note in Figure 3A,B is the

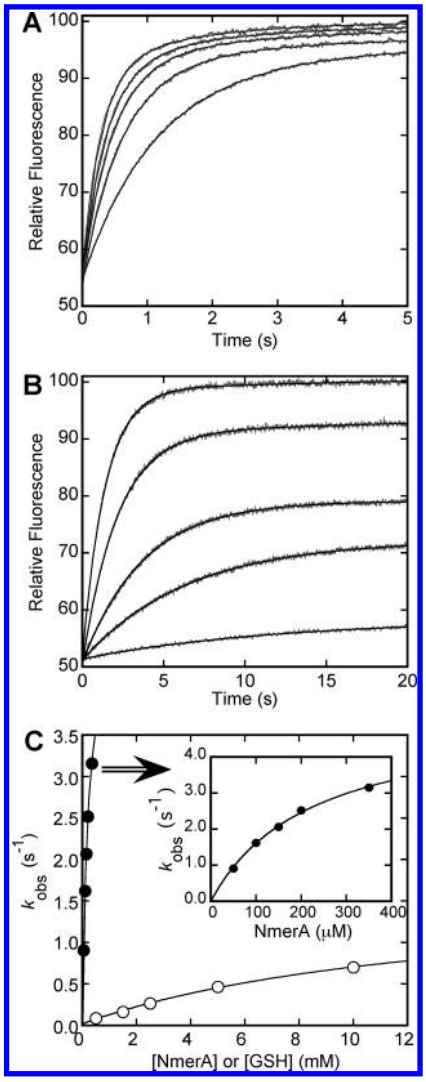

FIGURE 3: Stopped-flow kinetic analysis of Hg(II) transfer from HgMerB to the NmerA domain of MerA and glutathione. (A) Kinetic traces (from lower to higher) for reaction of 5 μM HgMerB with NmerA at 50, 100, 150, 200, and 350 μM, final concentrations. (B) Kinetic traces (from lower to higher) for reaction of 5 μM HgMerB with GSH at 0.5, 1.5, 2.5, 5, and 10 mM, final concentrations. Data in panels A and B are shown in dark gray; fits to eq 1 as described in the text are in black. (C) Observed first-order rate constants, k_{obs}, for the fast phases for Hg(II) removal from HgMerB as a function of NmerA or GSH concentration. Data for NmerA (●) and GSH (○) are compared in the main plot, and the NmerA data are expanded in the inset. The error bars are smaller than the symbols. Solid lines are the fits of the data to eq 2 in Kaleidagraph.

shorter time frame for the NmerA reactions, indicating they are much faster. This difference, along with the dramatic difference in concentrations yielding these rates, is emphasized in Figure 3C. Here the main plot shows a direct comparison of the observed rate constants (k_{obs}) obtained from the exponential fits to the traces in Figure 3A,B (see above), and the inset is an expansion of the NmerA data. Of particular interest, the observed rate even at the lowest concentration of NmerA examined here (50 μM) is faster than the rate with the highest concentration of glutathione (10 mM). This is significant because 50 μM is within the physiologically relevant range of full-length MerA (and hence NmerA) concentrations observed during Hg-stimulated expression of the pathway (*33*), while cellular glutathione concentrations are closer to 5 mM (*36*) and have been found to be significantly depleted in Hg-shocked cells (*37*).

Scheme 1: Minimal Mechanism Consistent with Concentration Dependence of k_{obs} for NmerA and GSH

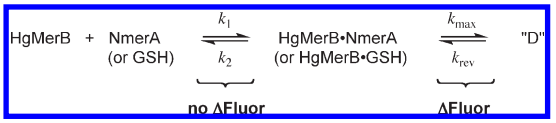

Analysis of the concentration dependence of the k_{obs} values in Figure 3C provides a further estimate of these differences. In both cases, the k_{obs} values exhibit a hyperbolic concentration dependence indicating the observed fluorescence change occurs in a rate-limiting first-order process after formation of an initial encounter complex between HgMerB and NmerA or GSH in a fluorescence-insensitive step. Qualitatively, this can be modeled by the minimal two-step mechanism in Scheme 1, where "D" may represent the fully dissociated MerB and HgNmerA or $Hg(SG)_2$ products or it may represent a combination of products and one or more intermediates that all have the same fluorescence properties as unliganded MerB. In either case, k_{max} provides an upper limit for the rate constant for removal of Hg(II) from MerB, while k_{rev} will only provide a qualitative indication of reversibility through the path from the fully dissociated MerB + Hg-dithiol products under the conditions evaluated here. A fit of k_{obs} to eq 2 (*29*), where B = NmerA or GSH, provides estimates for k_{max}, k_{rev}, and $K_{1/2} = (k_2 + k_{max})/k_1$, which is similar to a steady-state K_M, and the ratio of $k_{max}/K_{1/2}$ provides an apparent second-order rate constant as an estimate of the overall efficiency of the two species at removing Hg(II) from MerB. For NmerA, the fit to eq 2 yields $k_{max} = 5.23 \pm 0.22\ s^{-1}$, a k_{rev} value indistinguishable from 0, $K_{1/2} = 226 \pm 18\ \mu M$, and $k_{max}/K_{1/2} = (2.3 \pm 0.1) \times 10^4\ M^{-1}\ s^{-1}$. In contrast for GSH, k_{max} is lower at $1.63 \pm 0.26\ s^{-1}$, k_{rev} is $\sim 0.02\ s^{-1}$, and $K_{1/2}$ is drastically higher at 14 ± 4 mM, which is reflected in a much lower overall efficiency as measured by the $k_{max}/K_{1/2} = (1.2 \pm 0.2) \times 10^2\ M^{-1}\ s^{-1}$. Together, the combination of faster rates and highly favorable equilibria at low NmerA observed in these kinetic traces clearly indicates that direct Hg(II) transfer to NmerA will be the dominant pathway in vivo.

Although the two-step mechanism of Scheme 1 provides an accurate measure of the upper limits for the apparent first- and second-order rate constants for both reactions, the very low k_{rev} values are inconsistent with the incomplete reactions observed at the lowest NmerA concentration and all but the highest GSH concentration, indicating this simple two-step model does not adequately describe the full mechanism of either reaction. To address this, we evaluated chemically plausible expanded models for each reaction with global fits to the fluorescence traces using the software program Berkeley Madonna.

For the NmerA reaction, expansion of the simple model to include one additional step in the main reaction and a separate path for reaction of the minor species (Scheme 2) yields an excellent fit to all of the raw data traces (Figure 4A). In addition, the forward rate constant obtained for the slow step in this model, k_3, and the value of $K_{dNmerA} = k_2/k_1$ (Table 2) are very similar to the k_{max} and $K_{1/2}$ values obtained from analysis of the fast phase k_{obs} values with the two-step mechanism, indicating that inclusion of a slow interconversion of HgMerB·NmerA and MerB·HgNmerA between rapid equilibrium binding steps is sufficient to explain the observed equilibrium end point at low NmerA. In the working model in Scheme 2, we hypothesize that since the Hg(II) product is quite buried in the structure (Figure 2A), the slow step after NmerA binds may involve attack of Cys160 on

Scheme 2: Proposed Model for Reaction of NmerA with HgMerB

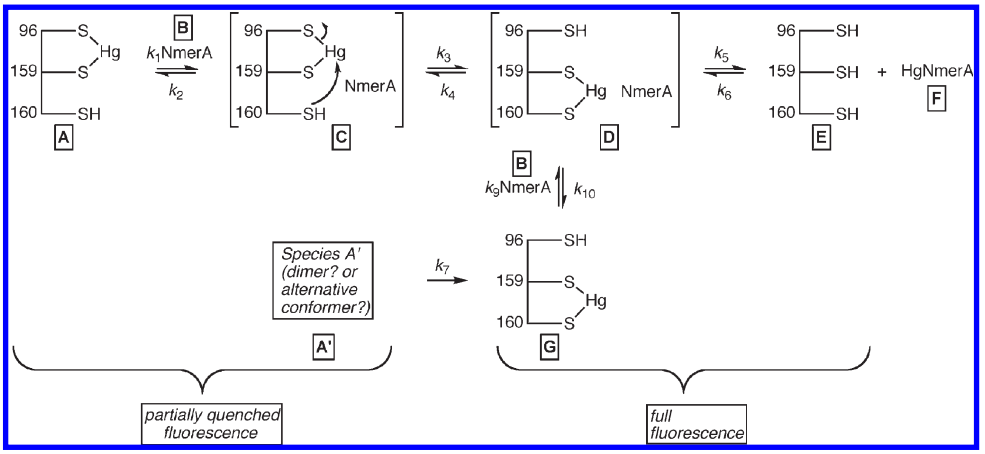

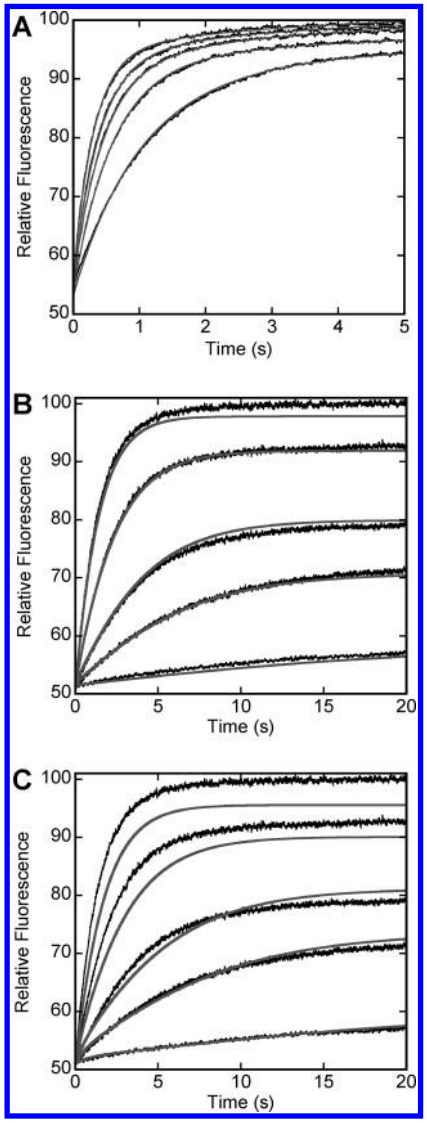

FIGURE 4: Berkeley Madonna global fits to kinetic traces for reactions of NmerA and GSH with HgMerB. (A) Fits for NmerA reactions using the model in Scheme 2. Final rate constants are summarized in Table 2. (B) Fits for GSH reactions using the full model in Scheme 3. Final rate constants are summarized in Table 3. (C) Fits for GSH reactions using the model in Scheme 3 with k_{17}, k_{18}, k_{19}, $k_{20} = 0$ to eliminate reversion path. Data in all panels are in black, and fits are in dark gray.

Table 2: Rate Constants for Fit of NmerA Traces to Full Model in Scheme 2

	Major Pathway	
k_1 (M^{-1} s^{-1})	7.4×10^5	$K_{dNmerA} = 195\ \mu M$
k_2 (s^{-1})	144	
k_3 (s^{-1})	5.2	
k_4 (s^{-1})	3.0	
k_5 (s^{-1})	330	$K_{dHgNmerA} = 660\ \mu M$
k_6 (M^{-1} s^{-1})	5.0×10^5	
	Minor Pathway	
k_7 (s^{-1})	0.30	
k_9 (M^{-1} s^{-1})	1.15×10^7	$K_{dNmerA} = 95\ \mu M$
k_{10} (s^{-1})	1082	

the Cys96−Hg−Cys159 complex to bring it to the protein surface where associated NmerA can rapidly extract it. Further examination of the kinetics of Hg(II) transfer from Cys160 and Cys96 mutants is underway to evaluate this hypothesis.

A key feature of the GSH reaction that is missing from the simple two-step model is the requirement for 2 equiv of GSH for complete removal of Hg(II) from MerB as $Hg(SG)_2$. The observation of monophasic fluorescence-sensitive changes with k_{obs} values showing only a hyperbolic dependence on GSH concentration indicates that the second GSH-dependent step occurs downstream of the fluorescence-sensitive step and is not rate-limiting. However, the presence of this step is expected to impact the overall equilibrium end points in a concentration-dependent manner. Scheme 3 shows chemically plausible pathways for transfer of Hg(II) among the MerB and GSH thiols with appropriate three-coordinate complexes known to occur during thiol ligand exchanges (*4*) included as important branch points for alternative paths of thiol dissociation. In this model, the rate-limiting step is proposed to be the fluorescence-insensitive attack of the first GSH (k_3) to form the first three-coordinate complex **D** that then rapidly equilibrates with the other two- and three-coordinate complexes downstream. The fluorescence-sensitive step is proposed to occur when Cys96 dissociates (as in the NmerA model) which here occurs in the subsequent rapid equilibrium conversion of species **D** to **F**. Comparison of the full model (Figure 4B) with a model excluding the path for dissociation of GSH from three-coordinate complex **G** (Figure 4C) indicates that inclusion of the path for reversion to **A** gives a remarkably good fit to both the apparent rate constants and the equilibrium end points in the data (Figure 4B). The rate constants

Scheme 3: Proposed Model for Reaction of GSH with HgMerB

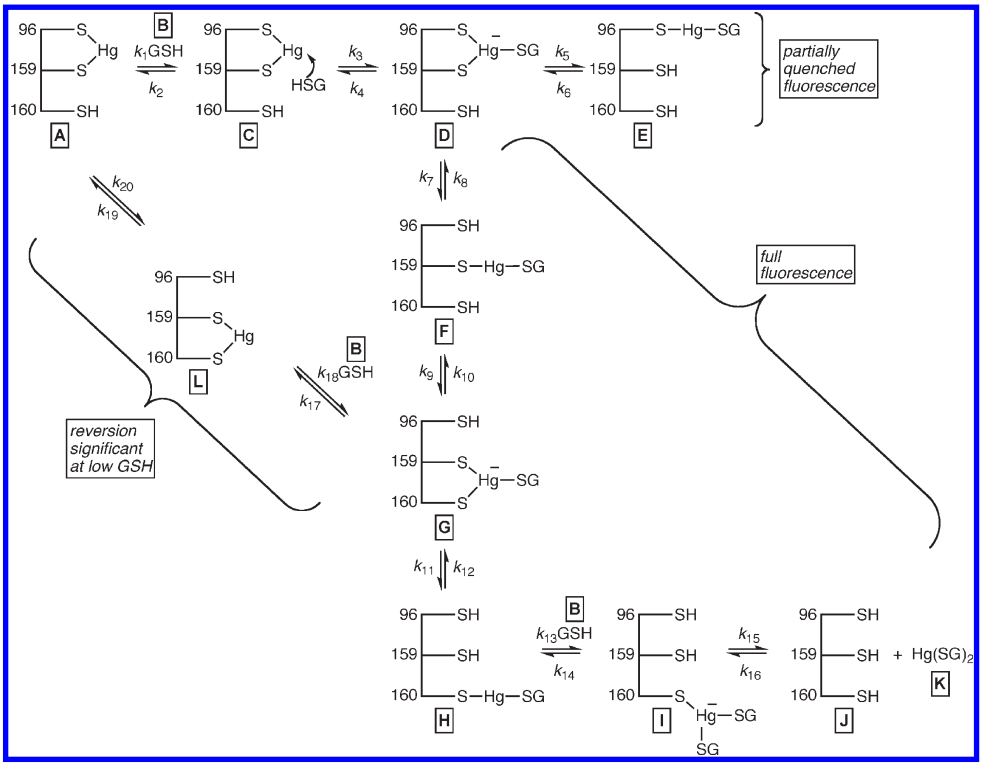

determined from the fit, although not likely to be a unique solution with a model this complex, are summarized in Table 3 and provide some insight into the relative K_d values for GSH and $Hg(SG)_2$ in the mechanism and the partitioning of intermediates needed to fit the data. Most important, the very weak initial association of GSH ($K_d \sim 18$ mM) and significant reversion to the starting HgMerB complex predicted by the model further emphasize the substantially lower efficiency of this monothiol in removing Hg(II) compared with the chelating NmerA.

MerA Catalytic Core Reacts Slowly with HgMerB Complex. Having established that direct transfer of Hg(II) from MerB to the NmerA domain is favored over transfer to GSH, the remaining question is whether NmerA is an essential mediator in the process for this class of MerB and MerA proteins or whether direct transfer of Hg(II) from MerB to the MerA catalytic core occurs just as efficiently. For this experiment, varying the MerA concentration while monitoring the change in fluorescence of the HgMerB complex is precluded by the high absorbance of the MerA protein and FAD cofactor ($\varepsilon_{280} \sim 70$ mM^{-1} cm^{-1}) (*26*) in the excitation window. However, we previously showed that with the inner cysteines oxidized and the C-terminal cysteines reduced the fluorescence of the FAD cofactor in MerA is sensitive to the ionization state of Cys464 (Cys558 in the full-length sequence) and can be used to monitor Hg(II) binding to the C-terminal cysteine pair (*14*). Thus, to measure the rates of Hg(II) transfer from the HgMerB complex to the MerA catalytic core, the concentration of the MerA core was fixed at 5 μM and the HgMerB complex was varied from 50 to 500 μM. At all concentrations, the FAD fluorescence increased very slowly, reaching a final end point consistent with complete transfer of Hg(II) from MerB to the MerA core (Figure 5). The traces fit best to a single exponential equation ($i = 1$ in eq 1), giving observed rate constants that vary linearly with [HgMerB] and yield a second-order rate constant of only 1.2×10^2 M^{-1} s^{-1} (Figure 5 inset). This is approximately 2 orders of magnitude lower than the apparent second-order rate constant for the transfer to NmerA ($k_{max}/K_{1/2} = 2.3 \times 10^4$ M^{-1} s^{-1}), providing strong evidence that NmerA is an essential mediator of the reaction in this class of MerB/MerA pairs.

Conclusions. In this study we directly evaluated the relative kinetic efficiencies of three potential pathways for Hg(II) transfer from the physiologically relevant HgMerB product complex to its coevolved MerA from a γ-proteobacterial *mer* locus. The results clearly establish (1) that direct handoff of Hg(II) between the proteins is highly favored both kinetically and thermodynamically over transfer to the competing cellular thiol glutathione at physiologically relevant concentrations of both and (2) that the more accessible cysteine pair in the N-terminal NmerA domain is the site for rapid Hg(II) transfer for this class of MerA/MerB pairs. The more favorable thermodynamics of the direct handoff is expected for the chelating cysteine pair in the NmerA domain versus a monothiol in competing glutathione and consistent with observations for other metal trafficking proteins (*9*−*11*). The more rapid kinetics for direct handoff to NmerA is also expected for an efficient detoxification pathway, but the fact that the Hg(II) product is completely buried in the HgMerB structure (Figure 2) indicates a conformational change in HgMerB must occur for the NmerA cysteine pair to access the Hg(II). Significantly, the hyperbolic dependence of the k_{obs} values on the NmerA concentration indicates that NmerA and HgMerB form a weak initial complex prior to the rate-limiting change in tryptophan fluorescence suggesting interaction with NmerA initiates the change. Recent results in our laboratory indicate that C160, located on a flexible loop with catalytic C159 (*18*), may be essential for access to bound Hg(II) by the cysteine pair of NmerA. Further studies of this process using MerB mutants are underway and will be reported elsewhere.

Our finding here that NmerA acquires Hg(II) from its coevolved HgMerB ~100-fold faster than the catalytic core C-terminal

Table 3: Rate Constants for Fit of GSH Traces to Full Model in Scheme 3[a]

	Main Path	
k_1 (M^{-1} s^{-1})	2.5×10^4	K_{d1GSH} = 17.7 mM
k_2 (s^{-1})	442	
k_3 (s^{-1})	2.16	
k_4 (s^{-1})	1.0	
k_5	0	
k_6	0	
k_7 (s^{-1})	87.6	
k_8 (s^{-1})	79.1	
k_9 (s^{-1})	81.4	
k_{10} (s^{-1})	96.4	
k_{11} (s^{-1})	77.2	
k_{12} (s^{-1})	109	
k_{13} (M^{-1} s^{-1})	4.75×10^4	K_{d2GSH} = 2.15 mM
k_{14} (s^{-1})	102	
k_{15} (s^{-1})	51	$K_{d1Hg(SG2)}$ = 0.51 mM
k_{16} (M^{-1} s^{-1})	9.99×10^4	
	Reversion Path	
k_{17} (s^{-1})	141	K_{d3GSH} = 3.36 mM
k_{18} (M^{-1} s^{-1})	4.2×10^4	
k_{19} (s^{-1})	42	K_{eq} = A/L = 190
k_{20} (s^{-1})	0.22	

[a]Species E was included in Scheme 3 as a plausible intermediate but was not included in the final fit since simulations with and without it did not alter the pattern of equilibrium end points.

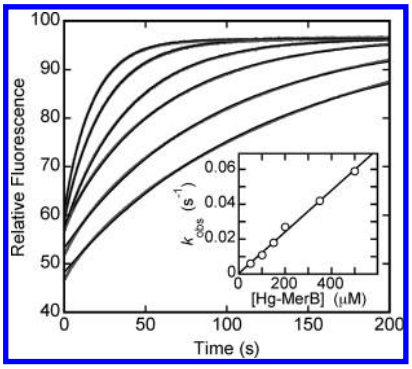

FIGURE 5: Stopped-flow kinetic analysis of Hg(II) transfer from HgMerB to the MerA catalytic core. Kinetic traces (from lower to higher) are for reaction of 5 μM MerA catalytic core with 50, 100, 150, 200, 350, and 500 μM HgMerB, final concentrations. Data are shown in dark gray; fits to eq 1 (i = 1) are in black. Inset: Observed first-order rate constants, k_{obs}, as a function of HgMerB concentration.

cysteine pair is consistent with our previous observations that NmerA can scavenge Hg(II) from cellular proteins such as thioredoxin much faster than the core (*13*), but the result is somewhat surprising in light of the fact that the core cysteine pair is completely conserved while NmerA is not. However, we have previously noted that the N-termini in MerA sequences appear to vary according to the cellular context and may be correlated with variations in their cellular thiol molecules (*7*). Of interest in the context of the current study, MerA from the broad spectrum locus from *Streptomyces lividans* (GenBank accession number X65467) (*38*), which uses mycothiol instead of glutathione (*39*), lacks an NmerA domain, and the sequence of its coevolved MerB (GenBank accession number X65467 (*38*)) also varies from the γ-proteobacterial MerB in its complement of cysteines, suggesting different mechanisms for Hg(II) transfer may have evolved for proteins from different loci due to such differences in their cellular environment. Further studies are underway to investigate this hypothesis.

ACKNOWLEDGMENT

We thank David Maltby for mass spectrometry analysis. We thank Drs. Cory Momany and Anne O. Summers for helpful discussion and for sharing their structural coordinates (PDB ID: 3FN8) for HgMerB before deposition.

SUPPORTING INFORMATION AVAILABLE

Figure S1, chromatograms of MerB and HgMerB taken as a function of time; Figure S2, chromatogram showing gel filtration separation of MerB/HgMerB and NmerA/HgNmerA from incubation of 1 molar equiv each of HgMerB and NmerA; Figure S3, ESI mass spectra for the NmerA/HgNmerA and MerB/HgMerB fractions obtained from the chromatographic separation; Figure S4, ESI mass spectra for NmerA and MerB. This material is available free of charge via the Internet at http://pubs.acs.org.

REFERENCES

1. Morel, F. M. M., Kraepiel, A. M. L., and Amyot, M. (1998) The chemical cycle and bioaccumulation of mercury. *Annu. Rev. Ecol. Syst. 29*, 543–566.
2. Clarkson, T. W., and Magos, L. (2006) The toxicology of mercury and its chemical compounds. *Crit. Rev. Toxicol. 36*, 609–662.
3. Casas, J. S., and Jones, M. M. (1980) Mercury(II) complexes with sulfhydryl containing chelating agents: stability constant inconsistencies and their resolution. *J. Inorg. Nucl. Chem. 42*, 99–102.
4. Cheesman, B. V., Arnold, A. P., and Rabenstein, D. L. (1988) Nuclear magnetic resonance studies of the solution chemistry of metal complexes. 25. $Hg(thiol)_3$ complexes and Hg(II)-thiol ligand exchange kinetics. *J. Am. Chem. Soc. 110*, 6359–6364.
5. Zalups, R. K., and Ahmad, S. (2005) Handling of cysteine S-conjugates of methylmercury in MDCK cells expressing human OAT1. *Kidney Int. 68*, 1684–1699.
6. Zalups, R. K., Aslamkhan, A. G., and Ahmad, S. (2004) Human organic anion transporter 1 mediates cellular uptake of cysteine-S conjugates of inorganic mercury. *Kidney Int. 66*, 251–261.
7. Barkay, T., Miller, S. M., and Summers, A. O. (2003) Bacterial mercury resistance from atoms to ecosystems. *FEMS Microbiol. Rev. 27*, 355–384.
8. Brown, N. L. (1985) Bacterial resistance to mercury—reductio ad absurbdum? *Trends Biochem. Sci. 10*, 400–403.
9. Banci, L., Bertini, I., Cantini, F., Massagni, C., Migliardi, M., and Rosato, A. (2009) An NMR study of the interaction of the N-terminal cytoplasmic tail of the Wilson disease protein with copper(I)-HAH1. *J. Biol. Chem. 284*, 9354–9360.
10. Gonzalez-Guerrero, M., and Arguello, J. M. (2008) Mechanism of Cu^+-transporting ATPases: soluble Cu^+ chaperones directly transfer Cu^+ to transmembrane transport sites. *Proc. Natl. Acad. Sci. U.S.A. 105*, 5992–5997.
11. Huffman, D. L., and O'Halloran, T. V. (2001) Function, structure, and mechanism of intracellular copper trafficking proteins. *Annu. Rev. Biochem. 70*, 677–701.
12. Ledwidge, R., Hong, B., Dötsch, V., and Miller, S. M. (2010) NmerA of Tn*501* Mercuric ion reductase: structural modulation of the pK_a values of the metal binding cysteine thiols (submitted).
13. Ledwidge, R., Patel, B., Dong, A., Fiedler, D., Falkowski, M., Zelikova, J., Summers, A. O., Pai, E. F., and Miller, S. M. (2005) NmerA, the metal binding domain of mercuric ion reductase, removes Hg^{2+} from proteins, delivers it to the catalytic core, and protects cells under glutathione-depleted conditions. *Biochemistry 44*, 11402–11416.
14. Ledwidge, R., Soinski, R., and Miller, S. M. (2005) Direct monitoring of metal ion transfer between two trafficking proteins. *J. Am. Chem. Soc. 127*, 10842–10843.

15. Rossy, E., Seneque, O., Lascoux, D., Lemaire, D., Crouzy, S., Delangle, P., and Coves, J. (2004) Is the cytoplasmic loop of MerT, the mercuric ion transport protein, involved in mercury transfer to the mercuric reductase? *FEBS Lett. 575*, 86–90.
16. Schue, M., Glendinning, K. J., Hobman, J. L., and Brown, N. L. (2008) Evidence for direct interactions between the mercuric ion transporter (MerT) and mercuric reductase (MerA) from the Tn*501* mer operon. *Biometals 21*, 107–116.
17. Schottel, J. L. (1978) The mercuric and organomercurial detoxifying enzymes from a plasmid-bearing strain of *Escherichia coli*. *J. Biol. Chem. 253*, 4341–4349.
18. Benison, G. C., Di Lello, P., Shokes, J. E., Cosper, N. J., Scott, R. A., Legault, P., and Omichinski, J. G. (2004) A stable mercury-containing complex of the organomercurial lyase MerB: catalysis, product release, and direct transfer to MerA. *Biochemistry 43*, 8333–8345.
19. Rossy, E., Champier, L., Bersch, B., Brutscher, B., Blackledge, M., and Coves, J. (2004) Biophysical characterization of the MerP-like amino-terminal extension of the mercuric reductase from *Ralstonia metallidurans* CH34. *J. Biol. Inorg. Chem. 9*, 49–58.
20. Griffin, H. G., Foster, T. J., Silver, S., and Misra, T. K. (1987) Cloning and DNA sequence of the mercuric- and organomercurial-resistance determinants of plasmid pDU1358. *Proc. Natl. Acad. Sci. U.S.A. 84*, 3112–3116.
21. Begley, T. P., Walts, A. E., and Walsh, C. T. (1986) Mechanistic studies of a protonolytic organomercurial cleaving enzyme: bacterial organomercurial lyase. *Biochemistry 25*, 7192–7200.
22. Begley, T. P., Walts, A. E., and Walsh, C. T. (1986) Bacterial organomercurial lyase: overproduction, isolation, and characterization. *Biochemistry 25*, 7186–7192.
23. Di Lello, P., Benison, G. C., Valafar, H., Pitts, K. E., Summers, A. O., Legault, P., and Omichinski, J. G. (2004) NMR structural studies reveal a novel protein fold for MerB, the organomercurial lyase involved in the bacterial mercury resistance system. *Biochemistry 43*, 8322–8332.
24. Lafrance-Vanasse, J., Lefebvre, M., Di Lello, P., Sygusch, J., and Omichinski, J. G. (2008) Crystal structure of the organomercurial lyase MerB in its free and mercury-bound form: insights into the mechanism of methylmercury degradation. *J. Biol. Chem. 284*, 938–944.
25. Pitts, K. E., and Summers, A. O. (2002) The roles of thiols in the bacterial organomercurial lyase (MerB). *Biochemistry 41*, 10287–10296.
26. Fox, B., and Walsh, C. T. (1982) Mercuric reductase-purification and characterization of a transposon-encoded flavoprotein containing an oxidation-reduction-active disulfide. *J. Biol. Chem. 257*, 2498–2503.
27. Miller, S. M., Moore, M. J., Massey, V., Williams, C. H., Jr., Distefano, M. D., Ballou, D. P., and Walsh, C. T. (1989) Evidence for the participation of Cys558 and Cys559 at the active site of mercuric reductase. *Biochemistry 28*, 1194–1205.
28. Bevington, P. R. (1969) Data Reduction and Error Analysis for the Physical Sciences, McGraw-Hill, New York.
29. Strickland, S., Palmer, G., and Massey, V. (1975) Determination of dissociation constants and specific rate constants of enzyme-substrate (or protein-ligand) interactions from rapid reaction kinetic data. *J. Biol. Chem. 250*, 4048–4052.
30. Schottel, J., Mandal, A., Clark, D., Silver, S., and Hedges, R. W. (1974) Volatilisation of mercury and organomercurials determined by inducible R-factor systems in enteric bacteria. *Nature 251*, 335–337.
31. Ogawa, H. I., Tolle, C. L., and Summers, A. O. (1984) Physical and genetic map of the organomercury resistance (Omr) and inorganic mercury resistance (Hgr) loci of the IncM plasmid R831b. *Gene 32*, 311–320.
32. Momany, C., Summers, A. O., Cagle, C., and Teske, J. PDB ID 3FN8 (unpublished data).
33. Summers, A. O. (1986) Organization, expression, and evolution of genes for mercury resistance. *Annu. Rev. Microbiol. 40*, 607–634.
34. Brown, N. L., Ford, S. J., Pridmore, R. D., and Fritzinger, D. C. (1983) Nucleotide sequence of a gene from the *Pseudomonas* transposon Tn*501* encoding mercuric reductase. *Biochemistry 22*, 4089–4095.
35. Engst, S., and Miller, S. M. (1999) Alternative routes for entry of HgX_2 into the active site of mercuric ion reductase depend on the nature of the X ligands. *Biochemistry 38*, 3519–3529.
36. Masip, L., Veeravalli, K., and Georgiou, G. (2006) The many faces of glutathione in bacteria. *Antioxid. Redox Signal. 8*, 753–762.
37. Lund, B. O., Miller, D. M., and Woods, J. S. (1993) Studies on Hg(II)-induced H_2O_2 formation and oxidative stress in vivo and in vitro in rat kidney mitochondria. *Biochem. Pharmacol. 45*, 2017–2024.
38. Sedlmeier, R., and Altenbuchner, J. (1992) Cloning and DNA sequence analysis of the mercury resistance genes of *Streptomyces lividans*. *Mol. Gen. Genet. 236*, 76–85.
39. Newton, G. L., Arnold, K., Price, M. S., Sherrill, C., Delcardayre, S. B., Aharonowitz, Y., Cohen, G., Davies, J., Fahey, R. C., and Davis, C. (1996) Distribution of thiols in microorganisms: mycothiol is a major thiol in most actinomycetes. *J. Bacteriol. 178*, 1990–1995.